HHS Public Access

Author manuscript

Alzheimers Dement. Author manuscript; available in PMC 2020 June 14.

Published in final edited form as:

Alzheimers Dement. 2020 June ; 16(6): 896–907. doi:10.1002/alz.12089.

Proteomic and Biological Profiling of Extracellular Vesicles from Alzheimer's Disease Human Brain Tissues

Satoshi Muraoka[1,*], **Annina M. DeLeo**[1,*], **Manveen K. Sethi**[2,*], **Kayo Yukawa-Takamatsu**[1], **Zijian Yang**[3], **Jina Ko**[3], **John D. Hogan**[4], **Zhi Ruan**[1], **Yang You**[1], **Yuzhi Wang**[1], **Maria Medalla**[5], **Seiko Ikezu**[1], **Mei Chen**[6], **Weiming Xia**[1,6], **Santhi Gorantla**[7], **Howard E. Gendelman**[7], **David Issadore**[3], **Joseph Zaia**[2], **Tsuneya Ikezu**[1,8,9,#]

[1]Department of Pharmacology and Experimental Therapeutics, Boston University School of Medicine, Boston, MA 02118, USA

[2]Department of Biochemistry, Boston University School of Medicine, Boston, MA 02118, USA

[3]Department of Bioengineering, University of Pennsylvania, Philadelphia, PA 19104, USA

[4]Program in Bioinformatics, Boston University, Boston, MA 02215, USA

[5]Department of Anatomy and Neurobiology, Boston University School of Medicine, Boston, MA 02118, USA

[6]Geriatric Research, Education and Clinical Center, Edith Nourse Rogers Memorial Veterans Hospital, Bedford, MA 01730, USA

[7]Department of Pharmacology and Experimental Neurosciences, University of Nebraska Medical Center, Omaha, NE 68198, USA

[8]Department of Neurology, Boston University School of Medicine, Boston, MA 02118, USA

[9]Center for Systems Neuroscience, Boston University, Boston, MA 2215.

Abstract

Introduction: Extracellular vesicles (EVs) from human Alzheimer's disease (AD) biospecimens contain amyloid-β peptide (Aβ) and tau. While AD EVs are known to affect brain disease pathobiology, their biochemical and molecular characterizations remain ill defined.

Methods: EVs were isolated from the cortical grey matter of 20 AD and 18 control brains. Tau and Aβ levels were measured by immunoassay. Differentially expressed EV proteins were assessed by quantitative proteomics and machine learning.

[#]**Correspondence author:** Tsuneya Ikezu, MD, PhD, Boston University School of Medicine, 72 East Concord St, L-606B, Boston, MA 02118, USA. tikezu@bu.edu Phone: 617-358-9575 Fax: 617-358-9574.

Author Contributions: S.M., A.M.D. and T.I. designed research; S.M., A.M.D., M.K.S., K.Y-T., Z.R., Y.Y., Y.W. and M.C. performed research; S.M., A.M.D., M.K.S., Z.Y., J.K., J.D.H., W.X., J.Z. and T.I. analyzed data; S.G. and H.E.G. provided brain samples; S.M. and T.I. wrote the paper; S.M., A.M.D., M.K.S., S.I., J.K., Z.Y., M.M., D.I., W.X., J.Z. and T.I. edited the paper.

[*]These authors contributed equally to this manuscript

Conflicts of Interest: TI collaborates with Abbvie Inc. (USA), Aethlone Medical, Inc. (USA), Eisai (Japan/USA) and Ono Pharmaceutical (Japan) and consults Takeda (Japan/USA).

Supplementary Data

The Supplementary data related to this article can be found as Supplementary Methods and Supplementary Data files.

Results: Levels of pS396 tau and Aβ1–42 were significantly elevated in AD EVs. High levels of neuron- and glia- specific factors are detected in control and AD EVs, respectively. Machine learning identified ANXA5, VGF, GPM6A and ACTZ in AD EV compared to controls. They distinguished AD EVs from controls in the test sets with 88% accuracy.

Discussion: In addition to Aβ and tau, ANXA5, VGF, GPM6A and ACTZ are new signature proteins in AD EVs.

Keywords

Alzheimer's disease; cortical grey matter; extracellular vesicles; microtubule-associated protein tau; amyloid beta peptide; proteome; machine learning

Background

Alzheimer's disease (AD) is the most common forms of dementia affecting nearly 50 million people worldwide. Neuropathologically, disease is characterized by amyloid plaques formed by extracellular aggregation of amyloid beta peptide (Aβ) and intracellular accumulation of neurofibrillary tangles (NFTs). These are formed in brain tissue by the hyperphosphorylated and misfolded microtuble-associated protein tau [1,2]. As AD progresses, Aβ and tau aggregates spread throughout the brain in a spatiotemporal manner [3,4]. Aβ deposition is most prominent in the frontal, anterior/posterior cingulate, lateral parietal and lateral temporal regions. Tau pathology, as classified by Braak and Braak, occurs in six histopathological stages. These correspond to tauopathy stages of AD. In stages I and II, NFTs appear in the entorhinal cortex and hippocampus,while in stage III and IV, higher densities extend beyond the entorhinal cortex and hippocampus to the neocortex. In the final V-VI stages, pathological tau deposits are present in throughout the hippocampus [3].

Extracellular vesicles (EVs), including exosomes (50-150nm), ectosomes/microvesicles (150-1000nm), and apoptotic bodies (1000-5000nm) are released from neurons, glia, and various other neural cells into the extracellular space [5-7]. These vesicles contain multiple forms of nucleic acids (microRNA, ncRNA, mRNA, DNA among others), lipids and proteins that are transferred from cell to cell, and found in blood, urine and cerebrosprinal fluid (CSF) [8,9]. In the central nervous system (CNS), it has been reported that AD-associated pathogenic proteins in brain EVs including tau and Aβ oligomers play important roles in AD pathogenesis [9-13]. Moreover, it has been reported that inhibition of EV synthesis reduced amyloid plaque deposition in the mouse model of AD, and stimulation of EV secretion increased intracellular transfer of prion protein in AD mouse models [10,11]. EVs are involved in the extracellular enzymatic degradation of Aβ and promote both Aβ aggregation and clearance by microglia [12,13]. Moreover, models of neuron-to-neuron transfer of tau seeds by EVs were reported [14-17]. Our own prior work demonstrated that microglia spread tau by EV secretion and that reducing EV synthesis significantly reduces tau propagation [18]. One mechanism centers around Bridging integrator 1 (BIN1), which is associated with the progression of tau pathology and observed by its abilities to alter tau clearance and by promoting the release of tau-enriched microglial EVs [19].

While EVs recovered from human and mouse brain tissues were examined by morphology, proteomics and RNA analyses [20-23], no comprehensive and quantitative proteomics database have yet been acquired for AD human brain tissues. Herein, we provide the first proteomic profiling of EVs isolated from postmortem AD and cognitively impaired control brain tissues . The analyses were combined with machine learning and quantitation of Aβ and tau species by epitope-specific ELISA. Machine learning identified and distinguished protein signatures of AD brain-derived EVs from controls with high degrees of accuracy.

Methods

Brain sample acquisitions

Two cohorts of brains were used in this study. The first cohort was obtained from the University of Nebraska Medical School (11 AD and 9 control) and the Greater Los Angeles Veteran's Affairs Hospital (9 AD and 9 control) as part of NIH NeuroBioBank, which were matched for age and sex. The second cohort was obtained from the NIH NeuroBioBank (22 AD and 18 control). All the AD and control cases were neuropathologically diagnosed and matched for age and sex. The Institutional Review Board at the University of Nebraska Medical School, Greater Los Angeles Veteran's Affairs Hospital and the NIH NeuroBioBank approved the brain acquisitions provided by informed consent.

Purification of EVs from human brain samples

0.5 g of largely grey matter tissue from the frontal cortex of deceased AD or control cases were processed for EV extraction based on reported method with some modifications (see supplementary file for detailed methods) [21].

Protein concentrations

The bicinchoninic acid (BCA) assay was used to determine protein concentration for each sample using Pierce BCA protein assay kit was used (# 23225 Pierce) (see supplementary file for detailed methods).

Enzyme-Linked Immunosorbent Assay (ELISA)

ELISAs were performed to assess levels of t-tau, p-tau, Aβ1-40 and Aβ1-42 and ANXA5 (see supplementary file for detailed methods).

Nanoparticle Tracking Analysis (NTA)

All samples were diluted in dfPBS at least 1:1000 or more to get particles within the target reading range for the Nanosight 300 machine (Malvern Panalytical Inc) (see supplementary file for detailed methods).

Transmission electron microscopy (TEM)

The EV isolated from AD or control brain tissue were analyzed by TEM (see supplementary file for detailed methods).

Mass spectrometry

The EV samples were subjected to chemical treatment, tryptic digenstion and liquid chromatography (LC)- electrospray ionization (ESI) tandem mass-spectroscopy (MS/MS) analysis (see supplementary file for detailed methods).

Sequence database

The raw LC-MS/MS data were converted into mZML format using ProteoWizard msConvert and analyzed using using PeaksDB and PeaksPTM using Peaks Studio version 8.0 (Bioinformatics Solutions, Inc., Waterloo, ON, Canada) against the Uniprot/Swissprot database for Homo sapiens with a 0.1% false discovery rate (FDR) and at least two unique peptides (see supplementary file for detailed methods) [24].

Statistical analyses

Statistical analysis was conducted using IBM SPSS software ver.25 and GraphPad Prism6. Between-group comparisons were analyzed by Student's t-test, nonparametric Mann-Whitney U, or one-way ANOVA followed by Bonferroni correction for multiple comparisons. The Gene Ontology of identified proteins were elucidated by DAVID Bioinformatics Resources 6.8. (https://david.ncifcrf.gov). The Venn diagram was generated using Venny_2.1 (http://bioinfogp.cnb.csic.es/tools/venny/).

Machine learning

The protein biomarkers to distinguish patients with Alzheimer's from controls were selected using Least Absolute Shrinkage and Selection Operator (LASSO) on the proteomics data from the training set (n = 21), where each patient's true state is labeled. An ensemble machine learning classifier to evaluate the performance of the selected proteins was developed as described (see supplementary file for detail methods) [25,26]. The machine learning generated model's performance was evaluated on a separate, user-blinded test set (n = 17).

Results

A total of 38 patient samples, composed of 20 AD (15M, 5F, Mean age: 75.0) and 18 control (14M, 4F, Mean age: 75.7) cases were used in study for EV biological and proteomics analyses A total of 78 patient samples, composed of 42 AD (25M, 17F, Mean age: 81.0) and 36 control (22M, 14F, Mean age: 79.0) cases, were included for validation analysis (Table 1). There were no statistical differences in the demographics between AD and controls with the exception of postmoterm intervals (PMI) of the validation set, which will be discussed in the validation study (Figure 4E).

Biochemical characterization of brain-derived EVs

The experimental workflow is summarized in Figure 1A. The EV samples were isolated from 20 AD and 18 sex- and age-matched cognitively unimpaired controls using the discontinuous sucrose gradient ultracentrifugation as previously described with modifications (see Materials and Methods). This technique of EV isolation has been

successfully used to isolate EVs from frozen mouse brain tissues [21,27]. In addition, we performed the quantitative proteomics analysis of human brain tissue homogenates and purified EV samples. The tetraspanins and ESCRT proteins were enriched in the EV samples, and contamination of non-EV molecules such as nucleus, mitochondria, ER and Golgi-related proteins as indicated in MISEV2018 guidelines [5] were diminished in the EV samples (Supplementary Table 1). To determine the purity of the EV preparations, EV samples were analyzed for their size and number by nanopariticle tracking analysis (NTA). The concentration of EVs derived from AD and control brains were not significantly different ($p = 0.6075$). The mode size distribution for EVs was significantly different and peaked at 122 nm for AD and 131 nm for controls ($p = 0.0095$) (Figure 1B). The EVs isolated from frozen brain tissue showed cap-shaped morphology by transmission electron microscopy (TEM) (Figure 1C). We next measured the concentration of total tau (t-tau) and p-tau at threonine 181 (pT181 tau), serine 199 (pS199 tau) and serine 396 (pS396 tau) in lysed EVs by ELISA. The levels of t-tau, pT181 tau, and pS199 tau showed no significant differences between AD and controls (t-tau: $p = 0.398$, pT181 tau: $p = 0.7235$, and pS199 tau: $p = 0.4384$) (Figure 1D and Supplementary Table 1). Conversely, pS396 tau was significantly increased in AD-brain derived EVs over controls (pS396 tau: $p = 0.0375$) (Figure 1D and Supplementary Table 1). Moreover, we observed a significant increase in Aβ1-42 in AD-derived EVs over controls ($p < 0.0001$), but not in Aβ1-40 ($p = 0.119$) (Figure 1E and Supplementary Table 1). The amount of pS396 and Aβ1-42 in the brain homogenate tissue were quantified by ELISA, and we performed the Bivariate correlation analysis between the homogenate samples and EV samples purified from the same AD brain samples. There is a significant difference in pS396 tau and Aβ1-42 levels in the brain tissue homogenate between AD and controls (pS396 tau; $p < 0.0001$, Aβ1-42; $p = 0.0001$). In additional, there is a significant positive correlation between the brain tissue homogenate and the EVs. The results suggest increased pS396 and Aβ1-42 level in the brain tissue might be related with elevation of pS396 and Aβ1-42 in the EVs (pS396; r = 0.4987, $p = 0.0050$, Aβ1-42; r = 0.5632, $p = 0.0005$) (Figure 1F).

Proteomic profiling of brain-derived EVs

We performed a label-free Nano-LC-MS/MS analysis of 38 EV samples for proteomic profiling. Across both cohorts, a total of 1,088 proteins were identified with at least two unique peptides (Figure 2A and Supplementary Table 3 and 4). There were 940 proteins identified in control EVs and 1,000 proteins identified in AD EVs. Among them, 852 proteins were detected in both groups, with 88 proteins unique to the controls and 148 proteins unique to the AD group (Figure 2A). The common, AD-unique and control-unique proteins were tested for properties pertaining to the ‘cellular component’ and ‘pathway’ ontologies by Gene Ontology analysis in the Database for Annotation, Visualization and Integrated Discovery (DAVID). Among the 852 shared proteins, 60.9% were found to be included in the extracellular exosome ontology (Figure 2B). The 148 proteins unique to the AD group were linked to mitochondria metabolism known to be dysfunctional in AD brain [28] (Figure 2B). Interestingly, in pathway analysis by DAVID, neurodegenerative disorders, including AD, Parkinson’s and Huntington’s diseases were enriched in common and unique proteins (Figure 2C). Figure 2D shows the peptides identified in AD group (not all AD patients) by Nano-LC-MS/MS, which covered 55.1% of tau (1-441), 9.1% of amyloid-beta

precursor protein (APP 1-770), 74.3% of alpha-synuclein (SNCA 1-140) and 6.3% of apolipoprotein E (APOE 1-317). Post-translational modification (PTM) analysis detected six phosphorylation sites (pT181, pS198, pS199, pS202, pT231, and pS404) on tau (Figure 2D, red bold letters). Notably, Aβ sequence was identified in APP fragments. Figure 2E shows the AD pathway from KEGG pathway analysis based on 68 proteins identified in the AD group, which are designated with red stars. The list of AD pathway-related proteins is provided in Supplementary Table 5. Proteins known to play an important role in AD pathogenesis, such as APP, APOE, tau and NADH-ubiquinone oxidoreductase (Cx I-V), were all identified in the AD group, although they were not unique to this group.

Analysis of label-free quantitative proteomics comparison of AD and control brain-derived EVs

Label-free quantitative proteomics analysis was performed using PEAKS studio software. A total of 949 proteins were quantified (Figure 3A and Supplementary Table 6). The 934 quantified proteins were common between AD and control groups. Between these groups, 3 proteins were uniquely expressed in the controls, while 12 proteins were uniquely expressed in the AD group. The principal component analysis (PCA) showed a marginal separation of the two groups (Figure 3B). Figure 3C shows the volcano plot of the common 289 proteins which were detected in more than 50% of the group (AD: $n > 10$ and controls: $n > 9$). Among these proteins, 15 proteins were significantly up-regulated and 3 proteins were significantly down-regulated in AD compared to the control group (as determined by $p < 0.05$ and $\log_2$ fold change threshold of > 1 or < -1) (Figure 3C and Table 2). The expression levels of 18 molecules identified in the AD group relative to the control group are displayed in a heatmap (Figure 3D). We next searched for brain cell-type specific molecules within the EV proteomics dataset using the mouse proteomics dataset as a reference [29]. The top 100 ranked cell type-specific molecules, which have at least 2-fold change in concentration in the cell type of interest over the other cell types, were tested with our EV proteomics dataset (Figure 3E). The distribution of these markers indicates that in the human brain, 49% of the identified molecules were related to neuronal origin, whereas other 50% of EV proteins are related to glial origin, including microglia, astrocytes and oligodendrocytes. Moreover, using label-free quantitative value, differences in the expression of cell type-specific marker molecules between AD and controls were seen (Figure 3F). Interestingly, neuron-specific molecules were enriched in the control group (Figure 3F, blue), while glia-specific marker molecules were enriched in the AD group (Figure 3F, red). These results suggest that glia may proliferate upon inflammatory response or accelerate their turnover, leading to enhanced generation of EVs in AD brains, which may be attributed to enhanced gliosis often seen in AD brains.

Machine learning to identify distinctive AD brain-derived EV proteins

To discover a combination of protein molecules that can accurately distinguish AD EVs from controls, the label-free quantitative proteomics dataset was analyzed using a machine learning method (Figure 4A). For this purpose, we split the proteomics dataset into an unblinded training subset (AD: $n = 11$; CTRL: $n = 10$) and a blinded testing subset (AD: $n = 9$; CTRL: $n = 8$). The ensemble machine learning model was built using only the data from the training subset, and then the accuracy of the diagnosis was determined using only the

blinded testing set. We found that a panel that included annexin-A5 (ANXA5), NGF-induced growth factor (VGF), neuronal membrane glycoprotein M6-a (GPM6A), and alpha-centractin (ACTZ), selected by the LASSO algorithm, resulted in an area under the ROC curve (AUC) of 0.95 within the training set (Figure 4B and Supplementary Table 7). We then examined the accuracy in the independent blinded test set using the 4 proteins in the dotted green box (Figure 4B). Using this model, we achieved an 88% accuracy (AUC = 0.97) in identifying AD patients using the panel that consisted of the four proteins (Figure 4C). Further, we ran two control experiments that randomly selected 4 proteins from a total possible 949 proteins to form the diagnosis panel (repeated 20 times, AUC = 0.58, Accuracy = 55%) and shuffling the true labels of the subjects within the training set (AUC = 0.47, Accuracy = 48%). The control's AUC was significantly worse than using the 4-protein panel's AUC ($P<0.001$) (Figure 4C). Figure 4D shows the scatter plot of 4 selected proteins, which were significantly differentially expressed between AD and control groups (Supplementary Table 8). Next, we assessed the correlation of expression of these candidate molecules to the levels of p-tau and Aβ1–42 in EVs by Pearson's correlation analysis. There was a significantly positive correlation between GPM6A and pS396 tau, and between GPM6A and Aβ1-42 levels (pS396 tau: r = 0.380, $p = 0.019$; Aβ1-42: r = 0.387, $p = 0.016$), and a significantly negative correlation between VGF and Aβ1-42 levels (r = −0.538, $p = 0.002$) (Figure 4E and Supplementary Table 9). ANXA5 expression level was significantly increased in AD brain-derived EVs compared to the control group in the validation cohort as determined by ELISA ($p = 0.0042$, 42 AD and 36 control cases, Figure 4F). Although there was statistical difference in PMI between AD and control cases in this cohort (Table 1), Pearson's correlation analysis of PMI and ANXA5 levels showed no significant correlation (r = −0.165, $p = 0.149$). Thus, this is not due to the difference in PMI between the two groups. Interestingly, ANXA5 expression level shows a tendency to increase along with Braak stages in an AD-dependent manner (Figure 4F). Therefore, ANXA5 is a potential EV molecule for both distinguishing AD and control EVs and as a surrogate marker for Braak stage.

Discussion

The biophysical properties of EVs isolated from unfixed postmortem human brain tissues, quantitative analysis of tau and Aβ species, and label-free quantitative proteomic profiling by Nano-LC-MS/MS analyses were performed. pS396 tau and Aβ1-42 levels were significantly increased in AD brain-derived EVs compared to controls. A total of 1,088 unique proteins from brain-derived EVs, were found to be enriched as extracellular exosomes molecules. We also quantified 949 proteins by label-free quantitative proteomic analysis, which were enriched in neuron-specific molecules in controls and glial cell type-specific molecules in the AD group. We used the feature selection algorithm LASSO to select a panel of protein biomarkers that could accurately diagnose AD, including ANXA5, VGF, GPM6A and ACTZ. It is important to note that the feature selection algorithm we used identifies the best panel of biomarkers for diagnosis, but is not necessarily a list of the most informative individual biomarkers. LASSO has the property that if there were, for example, two excellent biomarkers for AD, but which correlated highly one another, only one of these biomarkers would be included in the panel because including both would bring only

redundant information [30]. Using the validation cohort with the larger sample size, the increased protein level of ANXA5 in the AD group, as compared to controls was confirmed by ELISA.

Previous reports indicate pT181 tau to be an early PTM associated with AD, pS199 tau modification is thought to promote tau accumulation, and pS396 tau modification is associated with tau seeding activity and aggregation [31,32]. The PTM of tau at either pT181, pS199 or/and pS396 may facilitate the recruitment of tau in EVs, but neither pT181 nor pS199 tau is enriched in AD brain-derived EVs. This was unexpected since both pT181 and pS396 tau are elevated in neuron-derived exosomes in plasma samples obtained from AD and prodromal AD cases [33]. One potential explanation is that phosphorylation of specific sites on tau may be more preferentially incorporated into EV presumably via their ubiquitination, which is necessary for their MVB incorporation. In general, protein phosphorylation induces ubiquitination of lysine residues proximal to the phosphorylation sites, and it is necessary for ESCRT-mediated incorporation of ubiquitinated molecules into MVBs. Ubiquitination sites known for PHF-tau are K254, K311 and K353 [34], and phosphorylation of tau at S396 may facilitate its MVB sorting through ubiquitination of those lysine residues. In addition, we also observed tau fragments from the mid-region (156-406), which is inclusive of proline-rich domains (151-240), and microtubule binding repeat domains (24-369). Tau can be cleaved by various proteases including calpain-1 and 2 (at R230), thrombin, cathepsins, asparagine endopeptidase (at D255 and N368), caspase-2 (at D314) and caspase-3 (at D421) [35-38]. A further investigation is needed to determine how tau is truncated, phosphorylated and enriched in AD brain-derived EVs.

In the present study, we observed that the size of EVs derived from AD brain samples was smaller than from control EVs. It is possible that cholesterol level might be related to EV size, as small EVs contain significantly higher cholesterol than large EVs [39,40] and accumulation of cholesterol is associated with AD [41]. Enhancement of cholesterol levels increases Aβ production in cellular and animal models of AD, and inhibition of cholesterol synthesis reduces Aβ in this model [39-43]. Therefore, AD brain cells that accumulate high cholesterol might secrete smaller EVs than controls.

The GO of proteins identified in AD group showed mitochondria metabolism category. It is well known that mitochondrial dysfunction occurs in AD and by Aβ stimulation [44,45]. Recombinant tau mutant mimicking S396/S404 phosphorylation can enhance Aβ-induced mitochondrial damage and neuronal dysfunction [46], and mitochondrial dysfunction can be an upstream inducer of tau phosphorylation in AD [44]. In addition, mitochondrial dysfunction lead to their sorting to endolysosomal system and MVBs, which can release mitochondria-derived vesicles into the extracellular space as exosomes [47]. These reports suggest that Aβ accumulation induces mitochondrial dysfunction, increases tau phosphorylation at pS396 and enriches mitochondrial molecule in the EVs. Indeed, accumulation of misfolded proteins and mitochondrial dysfunction induces secretion of large vesicles (exophers) containing dysfunctional organelle and misfolded proteins for neuroprotection in *C. elegans* [48]. In terms of enriched ANXA5 in AD brain-derived EVs, the cellular apoptosis induced by mitochondrial dysfunction expresses phosphatidylserine on the cell surface and recruit ANXA5, which is a well-known phosphatidylserine binding

molecule. ANXA5-containing plasma membrane may be incorporated into the endosome, eventually to MVBs and secreted in EVs. There is, however, no literature to understand the connection between mitochondrial dysfunction and VGF, GPM6A or ACTZ.

The quantitative proteomic analysis of brain-derived EV samples isolated from AD and control patients found enriched glia-specific molecules in AD brain-derived EVs, and identified ANXA5, VGF, GPM6A and ACTZ as potential candidate molecules for monitoring the progression of AD. Although the Aβ and tau are tested for the diagnosis or progression of Aβ and tau pathology in AD, it may not cover atypical AD cases where A+T +N+ phenotype is incomplete. The four candidate molecules that would predict degenerative changes of neuronal and non-neuronal cells may facilitate the cellular based evaluation of the brain state in AD. Zhang *et al.* have recently reported that *ANXA5* is associated with familial late-onset AD by whole exome sequencing [49]. Further, Sohma *et al.* have reported a significantly higher plasma level of ANXA5 in AD cases compared to controls [50]. A number of previous studies in CSF and brain tissue have reported markedly lowered concentration of VGF in AD cases compared to controls [51-54]. GPM6A expression level was reported to be downregulated in the hippocampus of human AD brain tissues and transgenic AD mouse brains [55,56]. Since GPM6A homolog is located in neuropil in *D. melanogaster* [57], elevated GPM6A in AD brain EVs may be an indicator of the neuropil loss. Indeed, GPM6A is reported to clustered in lipid rafts upon palmitoylation, which are also enriched in sphingolipids and cholesterol [58]. Thus, reduction in GPM6A in brain tissue may be negatively correlated with GPM6A enrichment in EVs. In our study, ANXA5 was detected in brain-derived EVs from validation cohort, but VGF, GPM6A, and ACTZ were undetectable by commercial ELISA kits. Furhter study is necessary to validate these molecules with higher sensitivity ELISA. Finally, the combination of Aβ, tau and cell type-specific molecules from brain cells, including ANAX5, VGF, GPM6A or ACTZ may serve as potential biomarker candidate molecules in AD patient body fluid samples.

Supplementary Material

Refer to Web version on PubMed Central for supplementary material.

Acknowledgments

The authors thank Maria Ericsson (Electron Microscopy Facility, Harvard Medical School) for electron microscopic imaging services, participating laboratories of National Institute of Heatlh (NIH) NeuroBioBank for providing frozen human brain tissue specimens, and Li Wu (University of Nebraska Medical Center) for providing human brain tissue specimens.

Funding: This work is in part funded by Alzheimer's Association AARF-9550302678 (AMD & SM), DVT-14-320835 (TI), BrightFocus Foundation (A2016551S), Cure Alzheimer's Fund (TI), NIH R01 AG066429 (TI), RF1AG054199 (TI), NIH R56AG057469 (TI), NIH R01AG054672 (TI), NIH R21NS104609 (TI).

References

[1]. Goedert M, Wischik CM, Crowther RA, Walker JE, Klug A. Cloning and sequencing of the cDNA encoding a core protein of the paired helical filament of Alzheimer disease: identification as the microtubule-associated protein tau. Pnas 1988;85:4051–5. doi:10.1073/pnas.85.11.4051. [PubMed: 3131773]

[2]. Masters CL, Bateman R, Blennow K, Rowe CC, Sperling RA, Cummings JL. Alzheimer's disease. Nat Rev Dis Primers 2015;1:15056. doi:10.1038/nrdp.2015.56. [PubMed: 27188934]

[3]. Braak H, Braak E. Neuropathological stageing of Alzheimer-related changes. Acta Neuropathologica 1991;82:239–59. doi:10.1007/BF00308809. [PubMed: 1759558]

[4]. Thal DR, Rüb U, Orantes M, Braak H. Phases of A beta-deposition in the human brain and its relevance for the development of AD. Neurology 2002;58:1791–800. doi:10.1212/wnl.58.12.1791. [PubMed: 12084879]

[5]. Thery C, Witwer KW, Aikawa E, Alcaraz MJ, Anderson JD, Andriantsitohaina R, et al. Minimal information for studies of extracellular vesicles 2018 (MISEV2018): a position statement of the International Society for Extracellular Vesicles and update of the MISEV2014 guidelines. J Extracell Vesicles 2018;7:1535750. doi:10.1080/20013078.2018.1535750. [PubMed: 30637094]

[6]. You Y, Ikezu T. Emerging roles of extracellular vesicles in neurodegenerative disorders. Neurobiol Dis 2019;130:104512. doi:10.1016/j.nbd.2019.104512. [PubMed: 31229685]

[7]. Delpech J-C, Herron S, Botros MB, Ikezu T. Neuroimmune Crosstalk through Extracellular Vesicles in Health and Disease. Trends in Neurosciences 2019;42:361–72. doi:10.1016/j.tins.2019.02.007. [PubMed: 30926143]

[8]. Becker A, Thakur BK, Weiss JM, Kim HS, Peinado H, Lyden D. Extracellular Vesicles in Cancer: Cell-to-Cell Mediators of Metastasis. Cancer Cell 2016;30:836–48. doi:10.1016/j.ccell.2016.10.009. [PubMed: 27960084]

[9]. DeLeo AM, Ikezu T. Extracellular Vesicle Biology in Alzheimer's Disease and Related Tauopathy. J Neuroimmune Pharmacol 2018;13:292–308. doi:10.1007/s11481-017-9768-z. [PubMed: 29185187]

[10]. Guo BB, Bellingham SA, Hill AF. Stimulating the Release of Exosomes Increases the Intercellular Transfer of Prions. J Biol Chem 2016;291:5128–37. doi:10.1074/jbc.M115.684258. [PubMed: 26769968]

[11]. Dinkins MB, Dasgupta S, Wang G, Zhu G, Bieberich E. Exosome reduction in vivo is associated with lower amyloid plaque load in the 5XFAD mouse model of Alzheimer's disease. Neurobiol Aging 2014;35:1792–800. doi:10.1016/j.neurobiolaging.2014.02.012. [PubMed: 24650793]

[12]. Bulloj A, Leal MC, Xu H, Castaño EM, Morelli L. Insulin-degrading enzyme sorting in exosomes: a secretory pathway for a key brain amyloid-beta degrading protease. J Alzheimers Dis 2010;19:79–95. doi:10.3233/JAD-2010-1206. [PubMed: 20061628]

[13]. Yuyama K, Sun H, Mitsutake S, Igarashi Y. Sphingolipid-modulated exosome secretion promotes clearance of amyloid-β by microglia. J Biol Chem 2012;287:10977–89. doi:10.1074/jbc.M111.324616. [PubMed: 22303002]

[14]. Dujardin S, Bégard S, Caillierez R, Lachaud C, Delattre L, Carrier S, et al. Ectosomes: a new mechanism for non-exosomal secretion of tau protein. PLoS ONE 2014;9:e100760. doi:10.1371/journal.pone.0100760. [PubMed: 24971751]

[15]. Polanco JC, Li C, Durisic N, Sullivan R, Götz J. Exosomes taken up by neurons hijack the endosomal pathway to spread to interconnected neurons. Acta Neuropathol Commun 2018;6:10. doi:10.1186/s40478-018-0514-4. [PubMed: 29448966]

[16]. Wang Y, Balaji V, Kaniyappan S, Krüger L, Irsen S, Tepper K, et al. The release and trans-synaptic transmission of Tau via exosomes. Mol Neurodegener 2017;12:5. doi:10.1186/s13024-016-0143-y. [PubMed: 28086931]

[17]. Polanco JC, Scicluna BJ, Hill AF, Götz J. Extracellular Vesicles Isolated from the Brains of rTg4510 Mice Seed Tau Protein Aggregation in a Threshold-dependent Manner. J Biol Chem 2016;291:12445–66. doi:10.1074/jbc.M115.709485. [PubMed: 27030011]

[18]. Asai H, Ikezu S, Tsunoda S, Medalla M, Luebke J, Haydar T, et al. Depletion of microglia and inhibition of exosome synthesis halt tau propagation. Nat Neurosci 2015;18:1584–93. doi:10.1038/nn.4132. [PubMed: 26436904]

[19]. Crotti A, Sait HR, McAvoy KM, Estrada K, Ergun A, Szak S, et al. BIN1 favors the spreading of Tau via extracellular vesicles. Sci Rep 2019;9:9477. doi:10.1038/s41598-019-45676-0. [PubMed: 31263146]

[20]. Vella LJ, Scicluna BJ, Cheng L, Bawden EG, Masters CL, Ang C-S, et al. A rigorous method to enrich for exosomes from brain tissue. J Extracell Vesicles 2017;6:1348885. doi:10.1080/20013078.2017.1348885. [PubMed: 28804598]

[21]. Perez-Gonzalez R, Gauthier SA, Kumar A, Levy E. The exosome secretory pathway transports amyloid precursor protein carboxyl-terminal fragments from the cell into the brain extracellular space. J Biol Chem 2012;287:43108–15. doi:10.1074/jbc.M112.404467. [PubMed: 23129776]

[22]. Hurwitz SN, Sun L, Cole KY, Ford CR, Olcese JM, Meckes DG. An optimized method for enrichment of whole brain-derived extracellular vesicles reveals insight into neurodegenerative processes in a mouse model of Alzheimer's disease. J Neurosci Methods 2018;307:210–20. doi:10.1016/j.jneumeth.2018.05.022. [PubMed: 29894726]

[23]. Gallart-Palau X, Serra A, Sze SK. Enrichment of extracellular vesicles from tissues of the central nervous system by PROSPR. Mol Neurodegener 2016;11:41. doi:10.1186/s13024-016-0108-1. [PubMed: 27216497]

[24]. Adusumilli R, Mallick P. Data Conversion with ProteoWizard msConvert. Methods Mol Biol 2017;1550:339–68. doi:10.1007/978-1-4939-6747-6_23. [PubMed: 28188540]

[25]. Ko J, Baldassano SN, Loh P-L, Kording K, Litt B, Issadore D. Machine learning to detect signatures of disease in liquid biopsies - a user's guide. Lab Chip 2018;18:395–405. doi:10.1039/c7lc00955k. [PubMed: 29192299]

[26]. Ko J, Bhagwat N, Yee SS, Ortiz N, Sahmoud A, Black T, et al. Combining Machine Learning and Nanofluidic Technology To Diagnose Pancreatic Cancer Using Exosomes. ACS Nano 2017;11:11182–93. doi:10.1021/acsnano.7b05503. [PubMed: 29019651]

[27]. Silverman JM, Christy D, Shyu CC, Moon K-M, Fernando S, Gidden Z, et al. CNS-derived extracellular vesicles from superoxide dismutase 1 (SOD1)G93A ALS mice originate from astrocytes and neurons and carry misfolded SOD1. J Biol Chem 2019;294:3744–59. doi:10.1074/jbc.RA118.004825. [PubMed: 30635404]

[28]. Saman S, Lee NCY, Inoyo I, Jin J, Li Z, Doyle T, et al. Proteins recruited to exosomes by tau overexpression implicate novel cellular mechanisms linking tau secretion with Alzheimer's disease. J Alzheimers Dis 2014;40 Suppl 1:S47–70. doi:10.3233/JAD-132135. [PubMed: 24718102]

[29]. Sharma K, Schmitt S, Bergner CG, Tyanova S, Kannaiyan N, Manrique-Hoyos N, et al. Cell type- and brain region-resolved mouse brain proteome. Nat Neurosci 2015;18:1819–31. doi:10.1038/nn.4160. [PubMed: 26523646]

[30]. Zou H, Hastie T. Regularization and variable selection via the elastic net. Journal of the Royal Statistical Society: Series B (Statistical Methodology) 2005;67:301–20. doi:10.1111/j.1467-9868.2005.00503.x@10.1111/(ISSN)1467-9868.TOP_SERIES_B_RESEARCH.

[31]. Hanger DP, Anderton BH, Noble W. Tau phosphorylation: the therapeutic challenge for neurodegenerative disease. Trends Mol Med 2009;15:112–9. doi:10.1016/j.molmed.2009.01.003. [PubMed: 19246243]

[32]. Takeda S, Wegmann S, Cho H, DeVos SL, Commins C, Roe AD, et al. Neuronal uptake and propagation of a rare phosphorylated high-molecular-weight tau derived from Alzheimer's disease brain. Nat Commun 2015;6:8490. doi:10.1038/ncomms9490. [PubMed: 26458742]

[33]. Fiandaca MS, Kapogiannis D, Mapstone M, Boxer A, Eitan E, Schwartz JB, et al. Identification of preclinical Alzheimer's disease by a profile of pathogenic proteins in neurally derived blood exosomes: A case-control study. Alzheimers Dement 2015;11:600–1. doi:10.1016/j.jalz.2014.06.008. [PubMed: 25130657]

[34]. Cripps D, Thomas SN, Jeng Y, Yang F, Davies P, Yang AJ. Alzheimer disease-specific conformation of hyperphosphorylated paired helical filament-Tau is polyubiquitinated through Lys-48, Lys-11, and Lys-6 ubiquitin conjugation. J Biol Chem 2006;281:10825–38. doi:10.1074/jbc.M512786200. [PubMed: 16443603]

[35]. Rissman RA, Poon WW, Blurton-Jones M, Oddo S, Torp R, Vitek MP, et al. Caspase-cleavage of tau is an early event in Alzheimer disease tangle pathology. J Clin Invest 2004;114:121–30. doi:10.1172/JCI20640. [PubMed: 15232619]

[36]. Zhang Z, Song M, Liu X, Kang SS, Kwon I-S, Duong DM, et al. Cleavage of tau by asparagine endopeptidase mediates the neurofibrillary pathology in Alzheimer's disease. Nat Med 2014;20:1254–62. doi:10.1038/nm.3700. [PubMed: 25326800]

[37]. Kurbatskaya K, Phillips EC, Croft CL, Dentoni G, Hughes MM, Wade MA, et al. Upregulation of calpain activity precedes tau phosphorylation and loss of synaptic proteins in Alzheimer's disease brain. Acta Neuropathol Commun 2016;4:34. doi:10.1186/s40478-016-0299-2. [PubMed: 27036949]

[38]. Zhao X, Kotilinek LA, Smith B, Hlynialuk C, Zahs K, Ramsden M, et al. Caspase-2 cleavage of tau reversibly impairs memory. Nat Med 2016;22:1268–76. doi:10.1038/nm.4199. [PubMed: 27723722]

[39]. Durcin M, Fleury A, Taillebois E, Hilairet G, Krupova Z, Henry C, et al. Characterisation of adipocyte-derived extracellular vesicle subtypes identifies distinct protein and lipid signatures for large and small extracellular vesicles. J Extracell Vesicles 2017;6:1305677. doi:10.1080/20013078.2017.1305677. [PubMed: 28473884]

[40]. Pfrieger FW, Vitale N. Cholesterol and the journey of extracellular vesicles. J Lipid Res 2018;59:2255–61. doi:10.1194/jlr.R084210. [PubMed: 29678958]

[41]. Torres M, Busquets X, Escribá PV. Brain Lipids in the Pathophysiology and Treatment of Alzheimer’s Disease. Update on Dementia, InTech; 2016. doi:10.5772/64757.

[42]. Puglielli L, Tanzi RE, Kovacs DM. Alzheimer's disease: the cholesterol connection. Nat Neurosci 2003;6:345–51. doi:10.1038/nn0403-345. [PubMed: 12658281]

[43]. Evangelisti E, Cecchi C, Cascella R, Sgromo C, Becatti M, Dobson CM, et al. Membrane lipid composition and its physicochemical properties define cell vulnerability to aberrant protein oligomers. Journal of Cell Science 2012;125:2416–27. doi:10.1242/jcs.098434. [PubMed: 22344258]

[44]. Kerr JS, Adriaanse BA, Greig NH, Mattson MP, Cader MZ, Bohr VA, et al. Mitophagy and Alzheimer's Disease: Cellular and Molecular Mechanisms. Trends in Neurosciences 2017;40:151–66. doi:10.1016/j.tins.2017.01.002. [PubMed: 28190529]

[45]. Cadonic C, Sabbir MG, Albensi BC. Mechanisms of Mitochondrial Dysfunction in Alzheimer's Disease. Mol Neurobiol 2016;53:6078–90. doi:10.1007/s12035-015-9515-5. [PubMed: 26537901]

[46]. Quintanilla RA, Bernhardi von R, Godoy JA, Inestrosa NC, Johnson GVW. Phosphorylated tau potentiates Aβ-induced mitochondrial damage in mature neurons. Neurobiol Dis 2014;71:260–9. doi:10.1016/j.nbd.2014.08.016. [PubMed: 25134729]

[47]. Picca A, Guerra F, Calvani R, Bucci C, Monaco Lo MR, Bentivoglio AR, et al. Mitochondrial Dysfunction and Aging: Insights from the Analysis of Extracellular Vesicles. International Journal of Molecular Sciences 2017, Vol 18, Page 612 2019;20:805. doi:10.3390/ijms20040805.

[48]. Melentijevic I, Toth ML, Arnold ML, Guasp RJ, Harinath G, Nguyen KC, et al. C. elegans neurons jettison protein aggregates and mitochondria under neurotoxic stress. Nature 2017;542:367–71. doi:10.1038/nature21362. [PubMed: 28178240]

[49]. Zhang X, Zhu C, Beecham G, Vardarajan BN, Ma Y, Lancour D, et al. A rare missense variant of CASP7 is associated with familial late-onset Alzheimer's disease. Alzheimers Dement 2019;15:441–52. doi:10.1016/j.jalz.2018.10.005. [PubMed: 30503768]

[50]. Sohma H, Imai S-I, Takei N, Honda H, Matsumoto K, Utsumi K, et al. Evaluation of annexin A5 as a biomarker for Alzheimer's disease and dementia with lewy bodies. Front Aging Neurosci 2013;5:15. doi:10.3389/fnagi.2013.00015. [PubMed: 23576984]

[51]. Cocco C, D'Amato F, Noli B, Ledda A, Brancia C, Bongioanni P, et al. Distribution of VGF peptides in the human cortex and their selective changes in Parkinson“s and Alzheimer”s diseases. J Anat 2010;217:683–93. doi:10.1111/j.1469-7580.2010.01309.x. [PubMed: 21039478]

[52]. Llano DA, Devanarayan P, Devanarayan V, Alzheimer’s Disease Neuroimaging Initiative (ADNI). VGF in Cerebrospinal Fluid Combined With Conventional Biomarkers Enhances Prediction of Conversion From MCI to AD. Alzheimer Dis Assoc Disord 2019;Publish Ahead of Print:1. doi:10.1097/WAD.0000000000000328.

[53]. Hölttä M, Minthon L, Hansson O, Holmén-Larsson J, Pike I, Ward M, et al. An integrated workflow for multiplex CSF proteomics and peptidomics-identification of candidate

cerebrospinal fluid biomarkers of Alzheimer's disease. J Proteome Res 2015;14:654–63. doi:10.1021/pr501076j. [PubMed: 25490617]

[54]. Brinkmalm G, Sjödin S, Simonsen AH, Hasselbalch SG, Zetterberg H, Brinkmalm A, et al. A Parallel Reaction Monitoring Mass Spectrometric Method for Analysis of Potential CSF Biomarkers for Alzheimer's Disease. Proteomics Clin Appl 2018;12:1700131. doi:10.1002/prca.201700131.

[55]. Xu P-T, Li Y-J, Qin X-J, Scherzer CR, Xu H, Schmechel DE, et al. Differences in apolipoprotein E3/3 and E4/4 allele-specific gene expression in hippocampus in Alzheimer disease. Neurobiol Dis 2006;21:256–75. doi:10.1016/j.nbd.2005.07.004. [PubMed: 16198584]

[56]. Woo J-M, Park SJ, Kang HI, Kim BG, Shim SB, Jee SW, et al. Characterization of changes in global gene expression in the brain of neuron-specific enolase/human Tau23 transgenic mice in response to overexpression of Tau protein. International Journal of Molecular Medicine 2010;25:667–75. doi:10.3892/ijmm_00000390. [PubMed: 20372808]

[57]. Zappia MP, Bernabo G, Billi SC, Frasch AC, Ceriani MF, Brocco MA. A role for the membrane protein M6 in the Drosophila visual system. BMC Neurosci 2012;13:78–16. doi:10.1186/1471-2202-13-78. [PubMed: 22762289]

[58]. Ito Y, Honda A, Igarashi M. Glycoprotein M6a as a signaling transducer in neuronal lipid rafts. Neuroscience Research 2018;128:19–24. doi:10.1016/j.neures.2017.11.002. [PubMed: 29158160]

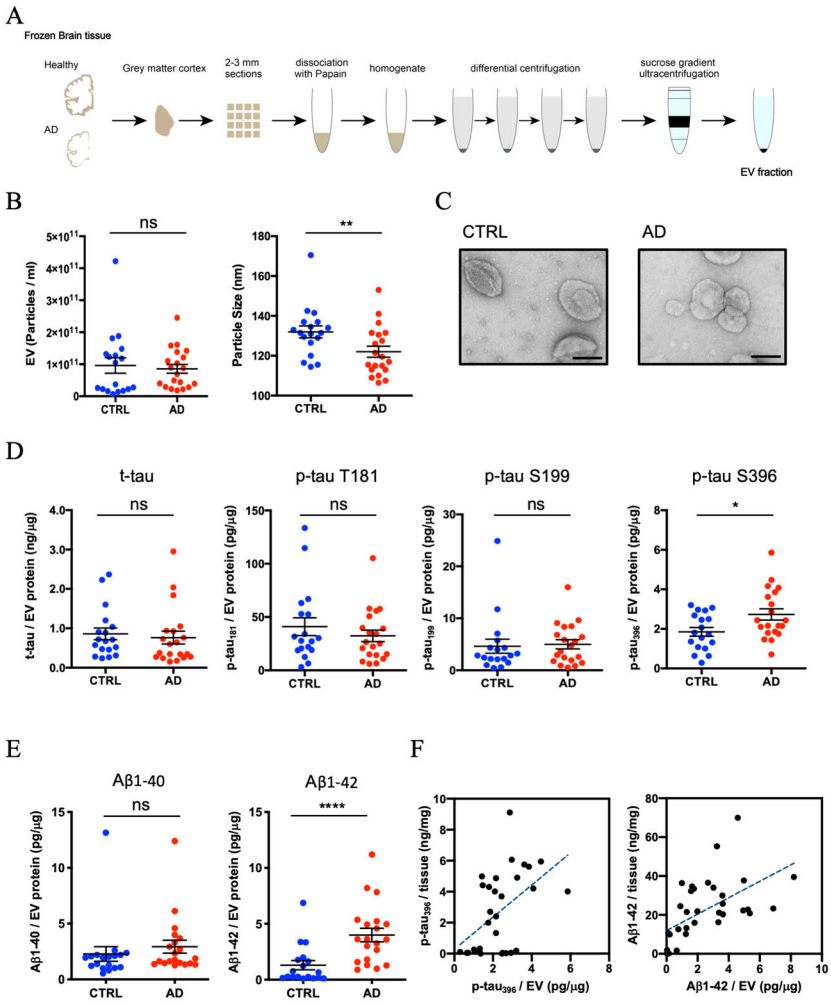

Figure 1. Biophysical and biochemical characterization of EVs isolated from AD and Control brain tissues:

A) Schematic of extracellular vesicle isolation protocol from human frozen brain tissue (see supplementary file for detailed methods). **B)** Left: Particle numbers of brain-derived EV fraction from control (CTRL) or AD by Nanoparticle tracking analysis. $p = 0.6075$ by Mann-Whitney test. Right: Particle size of brain-derived EV fraction. $p = 0.0095$ by Mann-Whitney test. **C)** TEM image of frozen human brain-derived EVs. Scale bar = 100 nm. Left: CTRL, Right: AD. **D)** Comparison of total tau and tau phosphorylated at threonine 181, serine 199, and serine 396 in EVs. pSer 396 tau; $p = 0.0375$ by Mann-Whitney test. **E)** Comparison of Amyloid beta 1-40 or 1-42 in EVs. Aβ1-42; $p < 0.0001$ by Mann-Whitney test. **F)** Scattered plot of brain tissue homogenates and brain-derived EVs. Left: pS396 tau (r = 0.4897, $p = 0.005$ using two-tailed t-test), Right: Aβ1-42 (r = 0.5632, $p = 0.0005$ using two-tailed t-test).

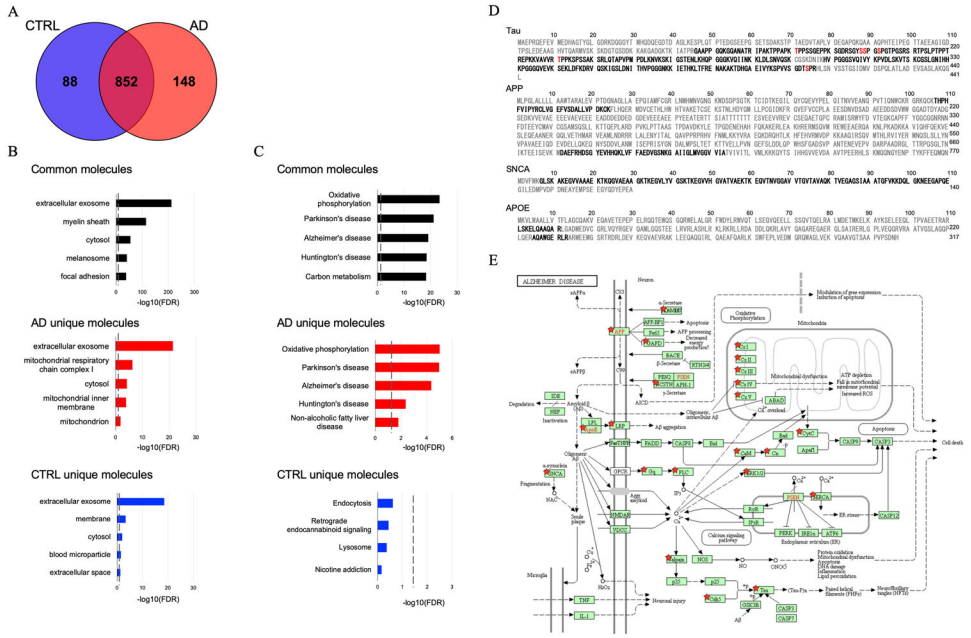

Figure 2. Proteomics profiling of EVs isolated from AD and CTRL brains:

A) Venn diagram representing the number of EV proteins differentially identified in CTRL and AD. **B)** Gene Ontology (GO) analysis using DAVID Bioinformatics Resources 6.8. The GO term of Top5 Cellular Component with $-\log_{10}$ (FDR *p*-value). **(C)** The GO term of Top5 Pathway Ontology with $-\log_{10}$ (FDR *p*-value). **D)** Sequence coverage of identified tryptic fragment peptide from Alzheimer's disease-related protein (Tau, APP, SNCA, APOE) in AD group by LC-MS/MS analysis. Identified peptides and phosphorylation sites are shown in black and red bold, respectively. **E)** KEGG pathway of Alzheimer Disease. The 68 proteins identified in the AD group are highlighted by red stars.

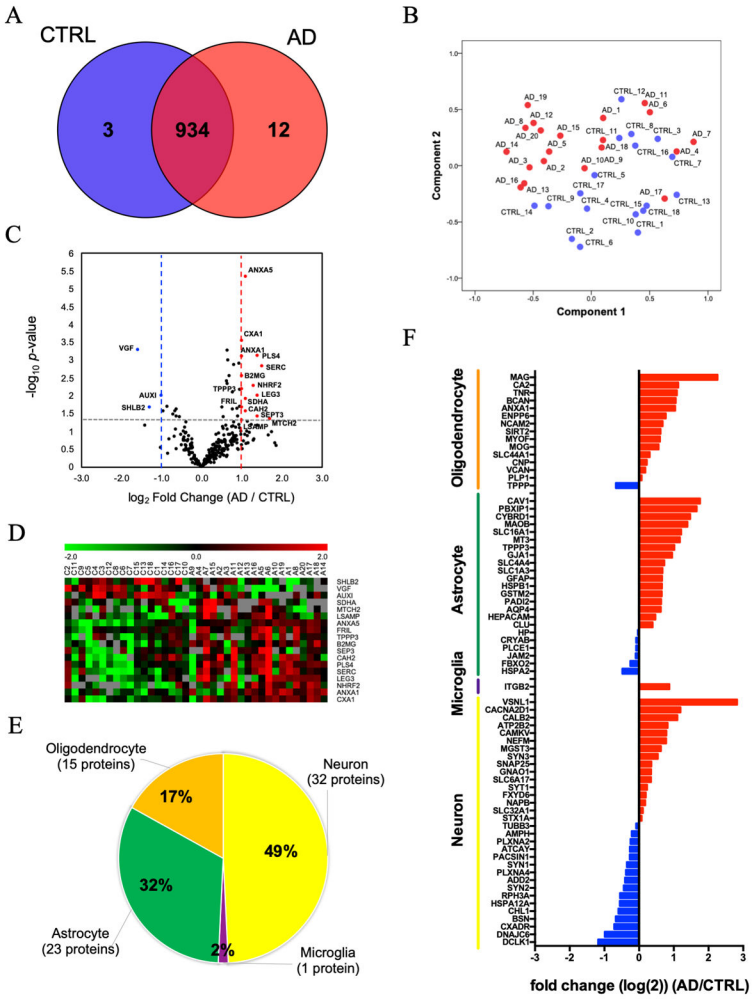

Figure 3. Label-free quantitative proteomics comparison of AD brain-derived EVs and CTRL brain-derived EVs:

A) Venn diagram representing the number of EV proteins differentially expressed in CTRL and AD. **B)** A principal component analysis (PCA). CTRL; blue symbols, AD; red symbols. **C)** Volcano plot showing a degree of differential expression of EV proteins in AD compared with CTRL. X-axis; log transformed fold change in expression, y-axis; log-transformed *p*-values. Grey dot lines: 0.1 *p*-value and 1- or −1-fold change cutoff **D)** Heat map representation of the up- and down-regulated proteins in AD. Red shows up-regulated proteins, and Green shows down-regulated proteins. **E)** Enrichment of brain cell type-specific markers in brain-derived EV proteins. Yellow: Neuron, Purple: Microglia, Green: Astrocytes, Orange: Oligodendrocytes. The parentheses show the number and percentage of identified cell type-specific protein. **F)** Comparison of the cell type-specific protein in AD brain-derived EV and CTRL EV. The red bar shows higher expression in AD. Blue bar indicates higher expression in CTRL.

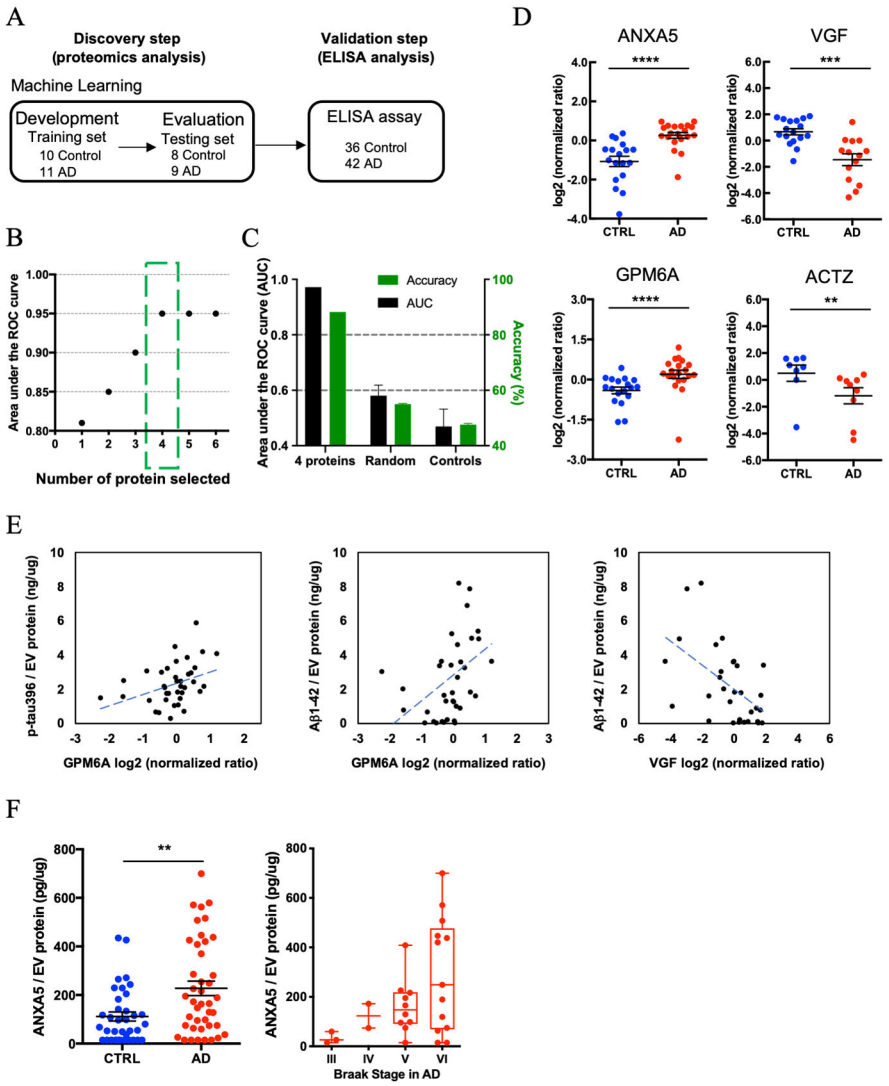

Figure 4. Machine learning model to identify AD brain-specific EV biomarker molecules:

A) Workflow for Machine learning approach. The training set is fed into linear discriminant analysis (LDA) to generate LDA vectors, which are applied to the blinded test set for classification. The predicted molecule are validated from the validation cohort by a commercial ELISA. **B)** The best performing panel based on the area under the ROC curve using the Lasso algorithm was selected in the training set. Y-axis; the area under the ROC curve, X-axis; proteins selected by the Lasso algorithm. The green box shows the selected protein with High AUC for the blinded test set. **C)** The Accuracy for 4 selected using the test set. Randomly selected control: Accuracy = 55%, AUC = 0.58., Shuffling control: Accuracy = 47.6%, AUC=0.47. **D)** A scatter plot of $\log_2$ (normalized ratio) as measured by proteomics per selected candidate protein in Machine Learning. (ANXA5: p = 4.58E-06, $\log_2$ fold change = 1.1, VGF: p = 5.30E-04, $\log_2$ fold change = −1.6, GPM6A: p = 5.37E-04, $\log_2$ fold change = 0.6, ACTZ: p = 4.44E-03, $\log_2$ fold change = −1.5). The t test was caluculated by Mann-Whitney test. **E)** Scattered plot of candidate molecules and AD pathogenic molecule in brain-derived EVs. Left: GPM6A and pS396 tau (r = 0.380, p = 0.019 using two-tailed t-

test). Center: GPM6A and Aβ1-42 (r = 0.387, $p = 0.016$). Right: VGF and Aβ1-42 (r = −0.538, $p = 0.002$). **F)** Left: Significant difference in total ANXA5 to total EV protein between AD and CTRL group by ELISA ($p = 0.0042$ by Mann-Whitney test) (AD = 42, CTRL = 36). Right: Braak stage-dependent increase in the ANXA5 expression level to total EV protein in AD dependent manner.

Table 1.

Patient information

Discoverer set			
For proteomics	**AD (n=20)**	**Control (n=18)**	***p*-value**[a]
Age, mean	75.0 ± 9.12	75.7 ± 8.88	0.997
Gender (male, female)	15M, 5F	14M, 4F	
PMI, mean	12.5 ± 8.68	17.8 ± 7.57	0.0675
Validation set			
For ELISA	**AD (n=42)**	**Control (n=36)**	***p*-value**
Age, mean	81.0 ± 11.64	79.0 ± 11.59	0.1533
Gender (male, female)	25M, 17F	22M, 14F	
PMI, mean	9.0 ± 7.25	17.3 ± 8.28	0.0069

[a]The statistical significance of the differences were calculated using Mann-Whitney test.

Table 2.

The list of up- and down- regulated protein in expression between AD and CTRL

UniProt ID	Protein name	$\log_2$(Fold Change) (AD/ CTRL)[a]	$-\log_{10}$(*p*-value)[b]
P08758	ANXA5	1.1	5.34
P17302	CXA1	1.0	3.54
O15240	VGF	−1.6	3.28
Q9NRQ2	PLS4	1.4	3.11
P04083	ANXA1	1.0	3.10
Q9Y617	SERC	1.5	2.83
P61769	B2MG	1.0	2.55
Q15599	NHRF2	1.3	2.27
Q9BW30	TPPP3	1.0	2.18
P17931	LEG3	1.4	2.00
O75061	AUXI	−1.0	2.00
P31040	SDHA	1.1	1.90
P02792	FRIL	1.0	1.67
Q9NR46	SHLB2	−1.3	1.67
P00918	CAH2	1.1	1.55
Q9UH03	SEPT3	1.4	1.42
Q9Y6C9	MTCH2	1.7	1.33
Q13449	LSAMP	1.0	1.30

[a]The $\log_2$ fold change were calculated by the protein intensity which was analyzed by PEAKS software.

[b]The statistical significance of the differences were calculated using Student's t test.